be used to determine their relative contributions to the oxygen fixed into cellulose.

The conclusion that the oxygen derived from CO_2 equilibrates with the oxygen of H_2O in the plant during the synthesis of cellulose indicates that the $\delta^{18}O$ value of cellulose is primarily a function of the oxygen isotopic composition of the H_2O in the plant. In similar fashion, the δD value of cellulose must be determined largely by the hydrogen isotopic composition of H_2O in the plant (*11*). Starting from the δD and $\delta^{18}O$ values of cellulose, the isotopic composition of the H_2O in a plant at the time the cellulose was formed can be reconstructed if the isotopic fractionations that occur during cellulose synthesis are known. It should also be possible to obtain a measure of the isotopic composition of the meteoric H_2O available to a plant from the values estimated for the isotopic composition of the H_2O in the plant, once the isotopic fractionations that occur during H_2O uptake are defined. The isotopic composition of meteoric H_2O can then be interpreted in terms of climatic temperature (*8, 9*), whereas the difference between the isotopic composition of meteoric H_2O and that of plant H_2O is due to the effects of evaporative transpiration and thus can serve as a measure of the humidity conditions under which the plant grew (*2, 16*). Realization of the full potential of isotopic analysis of cellulose for the purpose of climatic reconstruction requires a thorough understanding of the physical and chemical processes that influence its isotopic composition.

MICHAEL J. DENIRO
SAMUEL EPSTEIN
Division of Geological and Planetary Sciences, California Institute of Technology, Pasadena 91125

References and Notes

1. J. Gray and P. Thompson, *Nature (London)* **262**, 481 (1976).
2. S. Epstein, P. Thompson, C. J. Yapp, *Science* **198**, 1209 (1977).
3. C. D. Keeling, *Geochim. Cosmochim. Acta* **13**, 322 (1958); *ibid.* **24**, 277 (1961); Y. Bottinga and H. Craig, *Earth Planet. Sci. Lett.* **5**, 285 (1969).
4. For the standard experiment, we used commercial CO_2. For the ^{18}O-enriched experiment, an aliquot of CO_2 was equilibrated with H_2O containing 90 atom percent ^{18}O, then diluted with an excess of commercial CO_2.
5. L. E. Wise, *Wood Chemistry* (Reinhold, New York, 1944).
6. M. J. DeNiro and S. Epstein, in preparation.
7. ———, *Geochim. Cosmochim. Acta* **42**, 495 (1978).
8. I. Friedman, *ibid.* **4**, 89 (1953).
9. S. Epstein and T. Mayeda, *ibid.*, p. 213.
10. C. F. Bennett and T. E. Timell, *Sven. Papperstidn.* **58**, 281 (1955).
11. S. Epstein, C. J. Yapp, J. H. Hall, *Earth Planet. Sci. Lett.* **30**, 241 (1976).
12. $$\delta^*X = \left[\frac{(^*X/X)_{\text{sample}}}{(^*X/X)_{\text{standard}}} - 1\right] \times 1000$$
where *X and X are, respectively, the heavier and lighter isotopes of the element. The standards are standard mean ocean water (SMOW) for hydrogen and oxygen and the Peedee belemnite (PDB) carbonate for carbon.
13. The large standard deviations in the $\delta^{18}O$ values of the CO_2 used in the ^{18}O-enriched experiment are caused in part by the necessity of diluting these samples with large amounts of CO_2 of lower ^{18}O concentration before analyzing them in a mass spectrometer routinely used to measure $\delta^{18}O$ values of CO_2 samples of natural isotopic abundance.
14. J. R. O'Neil and S. Epstein, *J. Geophys. Res.* **71**, 4955 (1966). The difference between the $\delta^{18}O$ values of CO_2 and the H_2O with which it has completely equilibrated at 25°C is given by $40.73 + 0.04073\ \delta^{18}O_{H_2O}$.
15. There were three sources of H_2O within the box with which CO_2 could have exchanged. These were (i) the H_2O flowing through the box; (ii) the H_2O transpired by the plants and condensed out in the upper compartment of the box; and (iii) the H_2O in the plants, which could exchange with metabolic CO_2 that would subsequently be given off by the plants during respiration and photorespiration. In order to determine the extent of exchange between CO_2 and the H_2O flowing through the box, control experiments were carried out in which all flow conditions through the box were normal but neither plants nor corks were present. The $\delta^{18}O$ values of CO_2 in the air flowing into and out of the box during these control experiments were 916 ± 18 per mil ($N = 4$) and 573 ± 19 per mil ($N = 3$). Under the conditions of the growth experiments, with roughly half the holes in the perforated plate plugged with corks and the rest partially blocked with the shoots of plants (Fig. 1), the amount of this exchange would be reduced. The extent of exchange of CO_2 with H_2O condensed in the upper compartment of the box would increase during the course of the experiments, as the amount of H_2O transpired by the plants increased. In similar fashion, the amount of CO_2 given off during respiration and photorespiration would also increase during the course of the experiments, as the biomass of the plants increased. The combination of increases in these last two effects accounts for the observation that the $\delta^{18}O$ values of CO_2 in the air flowing out of the box, collected weekly during the last 3 weeks of each experiment, showed progressively larger effects of exchange. The $\delta^{18}O$ values for this CO_2 for the standard experiment were +30.6, +33.7, and +35.6 per mil; the corresponding values for the ^{18}O-enriched experiment were +186, +159, and +136 per mil.
The $\delta^{18}O$ values of the water flowing into and out of the box were virtually identical in each experiment. The oxygen isotopic composition of the H_2O supply was not affected by equilibration between CO_2 and H_2O because of the large ratio of H_2O to CO_2 in the box at any given time.
16. G. Dongman, H. Förstel, K. Wagener, *Nature (London) New Biol.* **240**, 127 (1972); J. Bricout, *J. Assoc. Off. Anal. Chem.* **56**, 739 (1973).
17. B. N. Smith and S. Epstein, *Plant Physiol.* **47**, 380 (1971).
18. The difference between the $\delta^{18}O$ values of H_2O distilled from the plants in the two experiments is due to isotopic exchange between oxygen of the H_2O and oxygen derived from the two CO_2 sources of markedly different ^{18}O contents. The value of 14.0 per mil represents an upper limit on the difference between $\delta^{18}O$ values of the plant H_2O, since the H_2O samples on which the measurements were made were collected when the amount of exchange was greater (since the relative humidity was higher, the transpiration rate was lower and thus the residence time of H_2O in the plants was longer) than at any other time during the experiments.
19. M. Calvin and J. A. Bassham, *The Photosynthesis of Carbon Compounds* (Benjamin, New York, 1962).
20. D. Samuel and B. L. Silver, *Adv. Phys. Org. Chem.* **3**, 123 (1965).
21. One part of the nutrient solution described by R. Y. Yih and H. E. Clark [*Plant Physiol.* **40**, 312 (1965)], to which disodium dihydrogen ethylenediaminetetraacetate was added to a final concentration of $1.8 \times 10^{-5}M$, was diluted with 2.79 parts of distilled H_2O before use.
22. We thank C. Kendall and S. N. Kurisu for technical assistance and R. H. Becker, J. Bonner, W. H. Klein, and R. M. Potter for discussions. This study was supported by NSF grant ATM76-03972. Contribution 3130 of the Division of Geological and Planetary Sciences, California Institute of Technology.

31 July 1978; revised 8 January 1979

The Moon: Sources of the Crustal Magnetic Anomalies

Abstract. *Previously unmapped Apollo 16 subsatellite magnetometer data collected at low altitudes over the lunar near side are presented. Medium-amplitude magnetic anomalies exist over the Fra Mauro and Cayley Formations (primary and secondary basin ejecta emplaced 3.8 to 4.0 billion years ago) but are nearly absent over the maria and over the craters Copernicus, Kepler, and Reiner and their encircling ejecta mantles. The largest observed anomaly (radial component ~ 21 gammas at an altitude of 20 kilometers) is exactly correlated with a conspicuous light-colored deposit on western Oceanus Procellarum known as Reiner γ. Assuming that the Reiner γ deposit is the source body and estimating its maximum average thickness as 10 meters, a minimum mean magnetization level of $5.2 \pm 2.4 \times 10^{-2}$ electromagnetic units per gram, or ~ 500 times the stable magnetization component of the most magnetic returned sample, is calculated. An age for its emplacement of ≤2.9 billion years is inferred from photogeologic evidence, implying that magnetization of lunar crustal materials must have continued for a period exceeding 1 billion years.*

A fundamental issue in the interpretation of lunar magnetism has been the identity of those the crustal materials that are magnetized to sufficient levels to produce the orbital anomalies (*1*). Previous investigations of these anomalies, using Apollo 15 and Apollo 16 subsatellite magnetometer data, were restricted to the 3 or 4 days per month when the moon was in the magnetically quiet environment of the geomagnetic tail lobes (*2, 3*). Because of several unfortunate dynamical commensurabilities (including the equality of the lunar orbital and spin periods), the subsatellites always traversed nearly identical surface locations on successive lunations and useful selenographic coverage was limited to narrow bands at a minimum altitude of 65 km across the heavily cratered farside highlands. No coverage at low altitudes across the geologically well understood near side was available.

The lack of nearside maps and the proximity of many farside anomalies to large craters such as Van de Graaff led to early suspicions that cratering itself could be an important mechanism for the production of large anomalies (*4*). The idea was appealing since it was consistent with several relatively uncomplicated theories of lunar magnetism. For example, either shock-induced magnetization of the surrounding terrain at the instant of impact (*5*) or excavation of a topographic depression in otherwise uniformly magnetized crust (*6*) would give rise to crater-associated fields. However, later, more accurate mapping of the farside anomalies (*2*) showed that the "Van de Graaff anomaly" total field maximum was actually positioned between the craters Van de Graaff and Aitken. Quantitative modeling of farside crustal fields, assuming a surface-plate source geometry, strongly indicated that actual sources are not correlated with the larger craters of the region (*3*). Also, a study of electron reflectance maxima (which are generally correlated with surface field maxima) over the nearside maria found no apparent associations with mare craters (*7*).

In 1973, after studies of returned samples and surface-site magnetic field measurements, Strangway *et al.* (*8*) proposed that relatively strongly magnetized crater and basin ejecta materials are the sources. They based their opinion on (i) the high measured magnetizations of certain classes of impact-generated breccias and (ii) the large surface magnetic fields apparently associated with the Cayley plains unit at the Apollo 16 landing site.

In this report we present evidence that basin and crater ejecta deposits are indeed major sources of orbital anomalies. Impacts are responsible for the shocked and heated materials that are magnetized, but no large anomalies are produced in association with crater interiors. These results are obtained by considering the large amount of relatively noise-free and unexamined data collected at times when the moon was in the solar wind and the subsatellite was at a low altitude in the lunar wake. Only Apollo 16 data have thus far been studied in order to take advantage of the perilously low perilunes that characterized the mission and that invariably occurred within the wake. Steady ambient fields and low-frequency trends were removed from selected data segments by using a quadratic detrending procedure, as is done when analyzing large-scale geomagnetic anomaly data (*9*). Each component was plotted against longitude, and repeated patterns on successive, closely spaced orbits served to distinguish true lunar fields from external and induced fluctuations. Figure 1 shows the radial field component for one series of orbit segments.

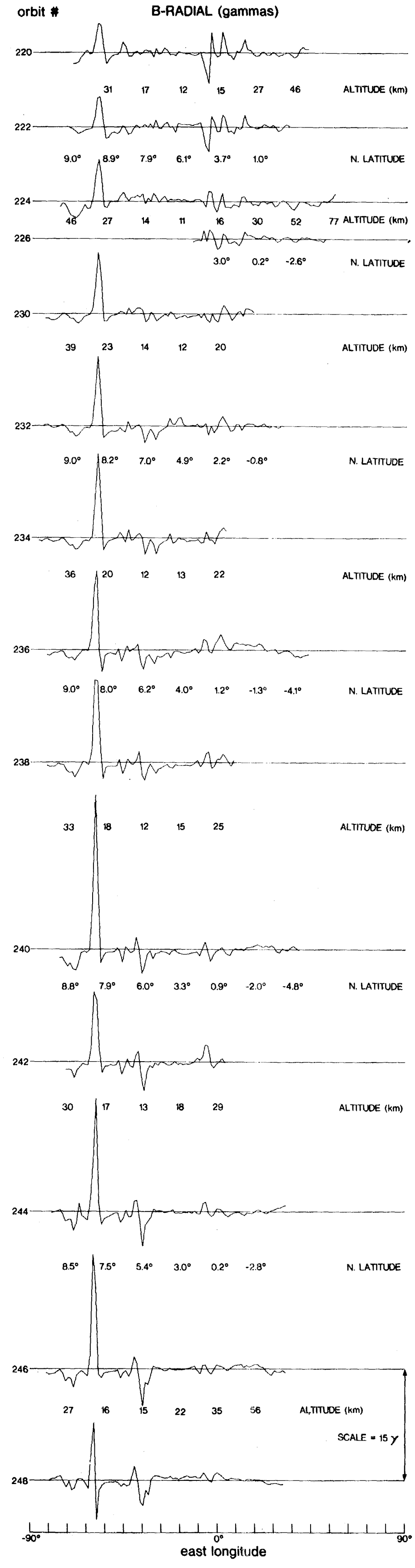

Fig. 1. Radial field component for a series of Apollo 16 subsatellite orbit segments plotted against longitude. Only times when the moon was in the solar wind but the subsatellite was in the lunar wake were selected to minimize contributions from external and induced fields. Latitude and altitude are indicated numerically below alternate data segments.

As expected, useful coverage was extended considerably, including for the first time a portion of the lunar near side at altitudes ranging from 11 to 50 km. Because of the small inclination (11°) of the subsatellite orbit plane to the lunar equator and to our selection of low-altitude wake segments only, latitudinal coverage was limited, extending at best from 3°S to 10°N. Similar procedures, if applied to data collected by a polar orbiting satellite, would allow almost global coverage.

As shown in Fig. 1, anomalies are present at nearly all points along the orbit tracks but they generally increase in both amplitude and complexity with decreasing altitude, indicating localized, near-surface sources. We have plotted on a map of the near side the orbit tracks shown in Fig. 1 as well as those of other usable Apollo 16 subsatellite orbits having low-altitude coverage. Figure 2 shows a comparison of one radial component data segment to a photomosaic of part of the central near side on which the orbit track has been drawn. The generalized results obtained by correlating field maxima with surface morphology and geology, using all available data segments, may be summarized as follows.

1) Anomalies are depleted in intensity and are less numerous over mare units than over highlands.

2) Very few anomalies occur in the vicinities of the young (< 1 billion years old) craters Copernicus and Kepler and their accompanying ejecta mantles and ray materials despite the extremely low altitudes (minimum, 11 km) of the subsatellite over these structures. No detectable anomaly is present near the mare-aged crater Reiner and its ejecta mantle.

3) Numerous anomalies of medium amplitude are present over the Fra Mauro and Cayley Formations (*10*) where they have not been flooded by mare basalt flows.

The relative sparsity of anomalies over the maria is not surprising in view of studies of returned samples, which have yielded stable magnetization intensities for mare basalts that are typically several orders of magnitude less than those of some classes of highland breccias (*1*). The lack of anomalies associated with both young and old crater interiors at once eliminates direct shock magnetization or demagnetization (at least in the case of material immediately surrounding the primary impact point) and indicates that topographic control of major anomalies is unlikely. A corollary of the latter result is that the mare basalt flows are not likely to be uniformly magnetized. Finally, the apparent association of many field maxima with primary and secondary basin ejecta materials (*10*) suggests that basin ejecta deposits are major sources of orbital anomalies. Acquisition of either thermoremanence or shock remanence or both during formation in the presence of an ambient magnetic field is the least improbable explanation for their magnetism. To a lesser degree, crater ejecta materials should produce measurable fields at subsatellite altitudes but the encircling mantles usually do not produce prominent anomalies.

The largest single anomaly contained in the data set and shown in Fig. 1 may represent an unusual example of a highly magnetic crater ejecta deposit located at some distance from its point of origin. This anomaly has a maximum radial component amplitude of 21 gammas (1 gamma = 10^{-5} gauss) at an altitude of 20 km and is the largest in apparent magnitude (uncorrected for measurement altitude) found to date in the Apollo 15 and 16 data (*11*). Its location (58.8°W, 7.6°N) is well correlated with that of a conspicuous deposit of intermediate albedo [typically 0.08 to 0.09 (*12*)] on western Oceanus Procellarum called Reiner γ. To demonstrate this correlation, we passed all available orbit segments through a two-dimensional filtering program with a minimum passed wavelength of 1.25°. A contour plot of the resulting total field intensity is compared in Fig. 3 with a Lunar Orbiter IV high-resolution photograph (part of frame 157) placed on an identical grid of longitude and latitude.

If the deposit is indeed the source of the observed anomaly, the mean magnetization is significantly larger than that of any returned sample. To show this, we modeled the volume of Reiner γ, using a 13-sided polygonal plate with a shape chosen to approximate that of the main deposit and a mean thickness $\bar{t}$ much less than the subsatellite altitude. A maximum value of 10 m for $\bar{t}$ is deducible from the absence of shadows cast by any part of the deposit under low sun illumination (*13*). Using the method of Talwani (*14*), we calculated anomalies producible by the volume of material at the subsatellite altitude for various assumed magnetization levels and directions. A single direction of magnetization for the entire deposit that closely reproduces the relative amplitudes and locations of maxima on the three vector component contour maps (not shown here) is radially outward and inclined 35° from the vertical toward the north. Assuming $\bar{t}$ = 10 m and a mean density for the source material of ~ 3 g/cm^3, we found that the mean magnetization required to match the observed anomaly amplitude is $5.2 \pm 2.4 \times 10^{-2}$ electromagnetic units (emu) per gram (*15*). For comparison, the stable magnetization component of the most magnetic of the returned samples has an intensity of about 10^{-4} emu/g (*1*).

A second result that follows from the identification of the anomaly with the Reiner γ deposit is that the magnetization of lunar crustal materials must have continued for a period exceeding 1 billion years. The Imbrium impact, which produced the magnetically prominent Fra Mauro Formation and may have produced part of the Cayley Formation (*10*), occurred about 3.9 to 4.0 billion years ago. The Orientale impact, which may otherwise have been responsible for the Cayley Formation, occurred 3.8 to 3.9 billion years ago (*16*). But the mare units on which much of the Reiner γ deposit is superposed have been dated by crater degradation measurements (*17*) and extrapolations of absolute ages ob-

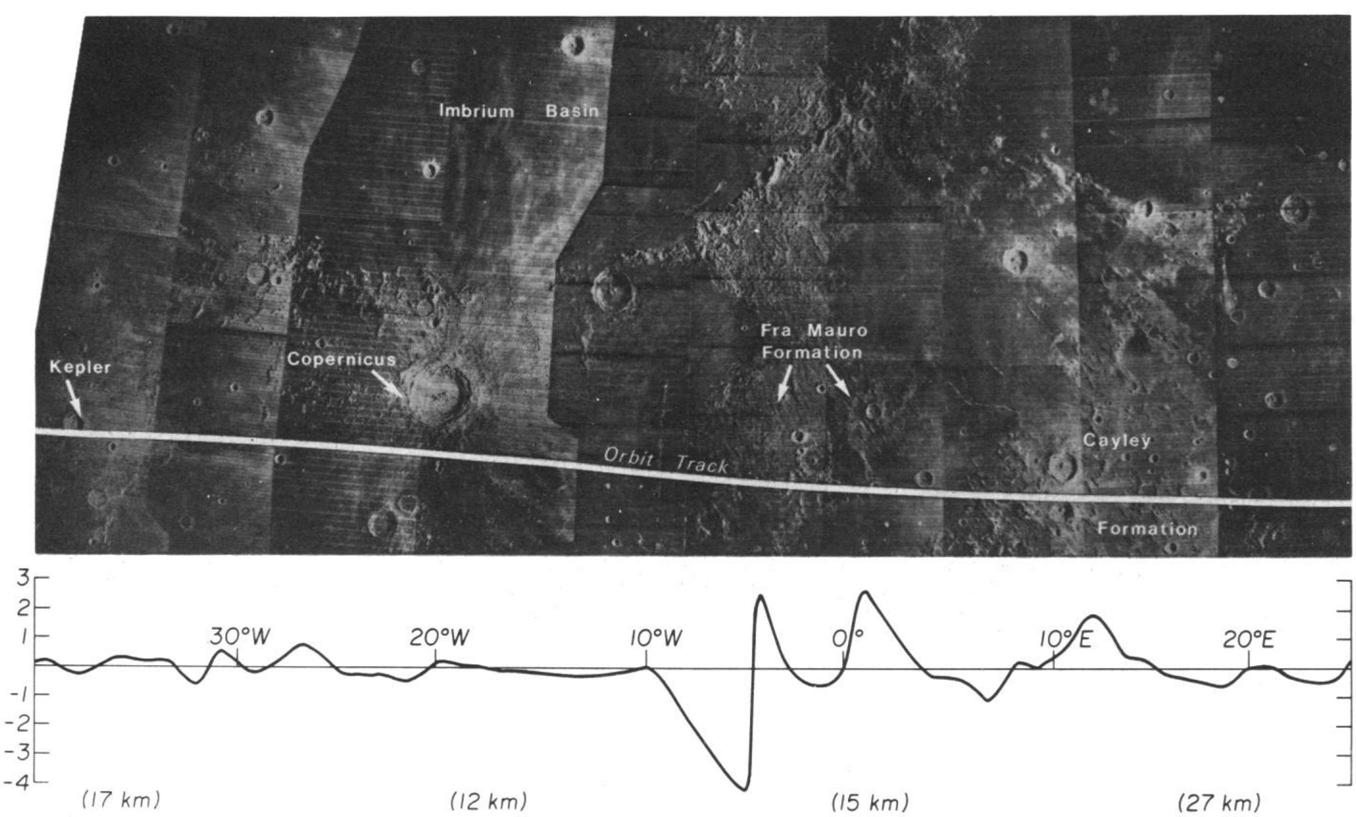

Fig. 2. Comparison of a radial component segment of orbit 220 (at the top in Fig. 1) with a Lunar Orbiter IV photomosaic of the central near side on which the orbit ground track has been drawn. The altitude of the subsatellite above the lunar surface is indicated at intervals beneath the plot. The impact that produced the Imbrium basin is responsible for the Fra Mauro Formation and may be at least partially responsible for the Cayley Formation. Magnetic anomalies appear to be associated with each of these geologic units but are nearly absent over the craters Copernicus and Kepler and their associated ejecta mantles despite the low altitudes achieved by the subsatellite. (One degree of longitude at the equator ≅ 30.3 km.)

tained from lunar samples elsewhere at 2.6 ± 0.3 billion years (*18*). The relatively high raylike albedo of Reiner γ and associated markings furthermore suggest Copernican age ($\lesssim$ 1 billion years old), but at least it is safe to conclude that they were formed some time after 2.9 billion years ago.

A much more difficult but an important problem is the origin of the deposit. If Reiner γ is Copernican, then only the solar wind field, which is now quite weak (~ 6 gammas), is likely to have been present at the time of its formation. If an ancient high-amplitude magnetic field magnetized Reiner γ in the same way that older nearside samples appear to have been magnetized (*1*), then its age must be near the estimated upper limit. Lunar stratigraphic relationships preclude a basin-related origin; therefore, if the deposit is either primary or secondary ejecta, some association with a large, postmare crater is indicated. There are two likely candidates (*19*). Olbers A is late Copernican in age and lies about 400 km to the west-northwest. Cavalerius is Eratosthenian (*12*) (perhaps 2 to 3 billion years old) and lies 200 km to the west. The similarity in albedo of Reiner γ to Olbers A ray materials is evidence for origin by impact or deposition of ejecta from that crater. However, the existence of V-shaped patterns in and southwest of the main deposit (photos IV-157H and IV-162H) that appear to point directly toward Cavalerius could be evidence for a Cavalerius origin. Also, the long axis of the main deposit is more nearly radial to Cavalerius than to Olbers A. The existence of a small cluster of craters near the point of the large curved V pattern (photo IV-157) suggests that they and Reiner γ could be genetically related. One possibility is that interference between rising plumes of thinly divided ejecta from these adjacent secondaries resulted in a difference in concentration of the ejected material downrange and produced the observed pattern, as experimentally verified for V-shaped ridges associated with secondary craters (*20*). Furthermore, Reiner γ and associated markings appear to grade into the Cavalerius ejecta mantle (which is also superposed on the mare), where numerous secondaries with V-shaped ridges occur (photo IV-162H).

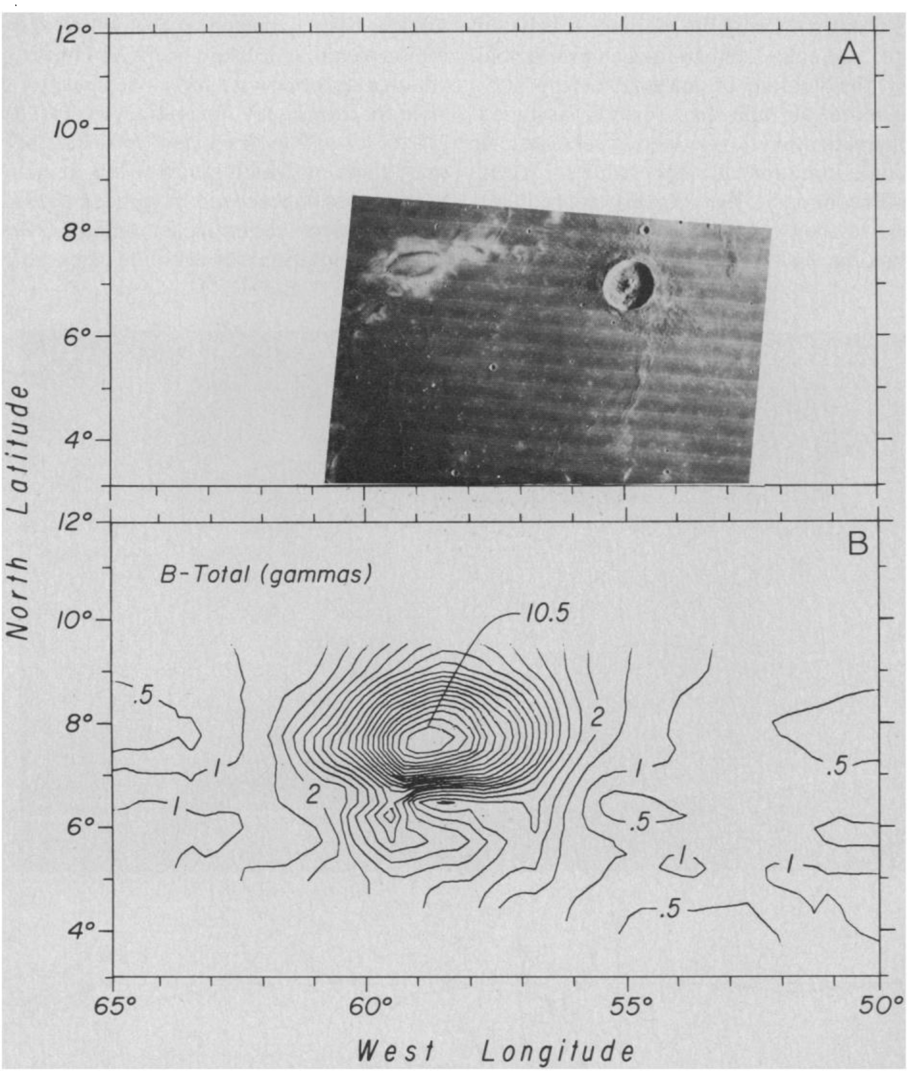

Fig. 3. (A) Section of Lunar Orbiter IV high-resolution frame 157 oriented with respect to a longitude-latitude grid by using McCauley's geologic map of the region (*12*) as a guide. (B) Two-dimensional contour map of the total magnetic field intensity based on available orbit segments. Although the altitude varies across the map, it is relatively constant (at about 20 km) near the center of the data swath. The offset of the largest anomaly peak from the center of mass of the entire elongated Reiner γ deposit (upper left corner of photo) is not larger than that expected from map control and tracking inaccuracies. A secondary maximum southwest of the largest peak appears to be correlated with a small associated swirl also southwest of the main deposit. There is no significant anomaly associated with the mare-aged crater Reiner (upper right corner of photo).

Finally, it is of interest to inquire whether Reiner γ-like deposits are found elsewhere on the moon and whether they have magnetics coverage. Similar relatively bright swirl-like deposits are present within southern Mare Ingenii on the far side and within a broad band across and north of Mare Marginis on the eastern limb (*19, 21, 22*). Unlike Reiner γ, these features do not appear to be linked by morphological characteristics to a particular local crater. The Ingenii deposits exist at such a high southern latitude (37°) that no magnetics coverage is available, but their location within 500 km of the large Van de Graaff–Aitken anomalies is noteworthy. Although no vector magnetometer data have yet been mapped over the Mare Marginis swirl belt, the electron reflectance map of the near side (*23*) shows a prominent region of high surface magnetic fields over roughly the same region. Thus, these Reiner γ-like features are candidates as sources for the observed large magnetic anomalies. The Van de Graaff–Aitken region and the area north of Mare Marginis are nearly antipodal to the Imbrium and Orientale basins, respectively, and are marked also by the occurrence of unusual hilly and lineated terrain (*22, 24*). The latter has been explained as due to compression by seismic waves generated by the basin impact (*25*) or by convergence of basin ejecta (*26*) at the antipode. There is therefore some evidence that the production of anomalously magnetic crater ejecta deposits has not been completely random in the highlands but may be related to special properties of the crust at the primary impact point.

In summary, a single hypothesis that is consistent with the subsatellite data as well as with studies of returned samples and surface magnetic fields is that basin and crater ejecta deposits are major sources of the orbital anomalies. The level of magnetization is weak peripheral to the impact region inside the crater, but it rises beyond the rim and may rise sharply in the case of some ejected materials transported ballistically to large distances. As the latter are probably also the materials most strongly shocked and heated by the impact event, a relative increase in the volume fraction of free iron grains capable of retaining a strong and stable magnetic remanence is to be expected (*1*).

L. L. HOOD
P. J. COLEMAN, JR.
Institute of Geophysics and Planetary Physics, University of California, Los Angeles 90024
D. E. WILHELMS
U.S. Geological Survey, Menlo Park, California 94025

References and Notes

1. D. Strangway, W. Gose, G. Pearce, J. Carnes, in *Magnetism and Magnetic Materials—1972*, C. Graham, Jr., and J. Rhyne, Eds. (American Institute of Phsics, New York, 1973), pp. 1178–1196; M. Fuller, *Rev. Geophys. Space Phys.* **12**, 23 (1974); P. Dyal, C. Parkin, W. Daily, *ibid.*, p. 568.
2. P. Coleman, Jr., and C. Russell, *Philos. Trans. R. Soc. London Ser. A* **285**, 489 (1977); C. Russell, P. Coleman, Jr., B. Fleming, L. Hilburn, G. Ioannidis, B. Lichtenstein, G. Schubert, *Proc. 6th Lunar Sci. Conf.* (1975), pp. 2955–2969; C. Russell, P. Coleman, Jr., G. Schubert, *Science* **186**, 825 (1974).
3. L. Hood, C. Russell, P. Coleman, Jr., *Proc. 9th Lunar Planet. Sci. Conf.* (1978), pp. 3057–3078.
4. P. Coleman, Jr., B. Lichtenstein, C. Russell, L. Sharp, G. Schubert, *Proc. 3rd Lunar Sci. Conf.* (1972), pp. 2271–2286; P. Coleman, Jr., C. Russell, L. Sharp, G. Schubert, *Phys. Earth Planet. Inter.* **6**, 167 (1972); P. Coleman, Jr., G. Schubert, C. Russell, L. Sharp, *NASA Spec. Publ. SP-289* (1971); *Moon* **4**, 419 (1972).
5. L. Srnka, *Proc. 8th Lunar Sci. Conf.* (1977), pp. 785–792.
6. S. K. Runcorn, *Phys. Earth Planet. Inter.* **10**, 327 (1975).
7. R. Lin, *Lunar and Planetary Science IX* (Lunar and Planetary Institute, Houston, 1978), pp. 651–653.
8. D. Strangway, W. Gose, G. Pearce, R. McConnell, *Nature (London)* **246**, 112 (1973).
9. R. Regan, *Geophys. Rev.*, in press.
10. The Fra Mauro Formation is a roughly textured blanket of debris deposited at the time of the Imbrium impact. The Cayley Formation is a smooth light plains unit found all around the moon but concentrated on the southern and southeastern periphery of the Fra Mauro Formation. It is believed to represent either direct deposition of ballistically transported ejecta from the Imbrium and Orientale events or indirect deposition of local materials due to secondary cratering at the time of these events. (*16*, pp. 37–39).
11. Assuming an (altitude)$^{-2.5}$ dependence as a first approximation indicates that the Reiner γ anomaly is the largest in absolute terms as well across the near side within the region of coverage. A number of farside anomalies, including those near the craters Van de Graaff and Aitken, appear to be as much as three to five times larger than the Reiner γ anomaly when scaled to a common altitude.
12. J. McCauley, *U.S. Geol. Surv. Map I-491* (1967).
13. According to D. W. G. Arthur (personal communication), mare ridges similar to those transecting the Reiner γ deposit have slopes 20 to 50 m high where they have been measured in other areas. The ridges that transect the deposit cast shadows on available telescopic photos (taken at low sun illumination angles) that show no shadows for the deposit itself. Additional visual searches (which have higher resolving power than photos under good conditions) also showed no shadows for the deposit. On this basis, a maximum *mean* thickness of 10 m is estimated.
14. M. Talwani, *Geophysics* **30**, 797 (1965).
15. The mean of the radial component for orbits 238, 240, and 242 (Fig. 1) was used to represent the maximum radial component amplitude of the anomaly. The error estimate is a reflection of the standard deviation from the mean for these three measurements.
16. S. R. Taylor, *Lunar Science: A Post-Apollo View* (Pergamon, New York, 1975), pp. 276–279.
17. L. Soderblom and L. Lebofsky, *J. Geophys. Res.* **77**, 279 (1972); L. Soderblom and J. Boyce, *NASA Spec. Publ. SP-315* (1972), pp. 29:3–29:6; J. Boyce and A. Dial, Jr., *Proc. 6th Lunar Sci. Conf.* (1975), pp. 2585–2595.
18. J. Boyce, *Proc. 7th Lunar Sci. Conf.* (1976), pp. 2717–2728. No samples were returned from western Oceanus Procellarum.
19. P. Schultz, *Moon Morphology* (Univ. of Texas Press, Austin, 1976), pp. 420–423.
20. V. Oberbeck and R. Morrison, *Moon* **9**, 415 (1974).
21. F. El-Baz, *NASA Spec. Publ. SP-315* (1972), pp. 29:93–29:97.
22. D. Wilhelms and F. El-Baz, *U.S. Geol. Surv. Map I-948* (1977).
23. Frontispiece, *Proc. 8th Lunar Sci. Conf.* (1977).
24. D. Stuart-Alexander, *U.S. Geol. Surv. Map I-1047* (1978).
25. P. Schultz and D. Gault, *Moon* **12**, 159 (1974).
26. H. Moore, C. Hodges, D. Scott, *Proc. 5th Lunar Sci. Conf.* (1974), pp. 71–100.
27. We thank C. T. Russell and H. Weiss for numerous helpful and informative discussions. Supported by NASA grant NGR-05-007-351.

5 December 1978

Fluidization: Hydrodynamic Stabilization with a Magnetic Field

Abstract. *Fluidization of magnetizable particles by a gas stream in the presence of a uniform applied magnetic field oriented parallel to the flow prevents the hydrodynamic instability that otherwise leads to bubbles and turbulent motion within the medium. The fluidized emulsion expands uniformly in response to gas flow speeds in excess of that at the incipient fluidization point, with transition from the quiescent stable state to bubbling occurring suddenly at a characteristic increased rate of flow. Experimental data demonstrate the dependence of this transition velocity on the intensity of the applied magnetic field, length of the bed, and type of magnetic solids. Data illustrate the pressure distribution through the bed medium, the bed flow characteristics, and other related phenomena.*

This report describes magnetic stabilization of the uniform flow of gas relative to fluidized solids under conditions where gas bubbles normally appear. Fluidized beds first became of major importance through the development of a fluidized process for cracking heavy hydrocarbon into petroleum naphtha (*1*), and many applications in fossil fuel conversion and other areas are foreseen.

The phenomenon of fluidization can be visualized in terms of the simple experiment depicted in Fig. 1A, where a bed of solid particles is supported on a horizontal porous grid in a vertical tube. Gas or liquid is forced to flow upward through this grid and so through the particle bed. The flow causes a pressure drop across the bed, and when the pressure drop is sufficient to support the weight of the particles, the bed is said to be incipiently fluidized. The fluidized bed thus formed has many of the properties of a liquid: objects float on the surface, and the addition or withdrawal of solid particles in process equipment is also facilitated (*2*).

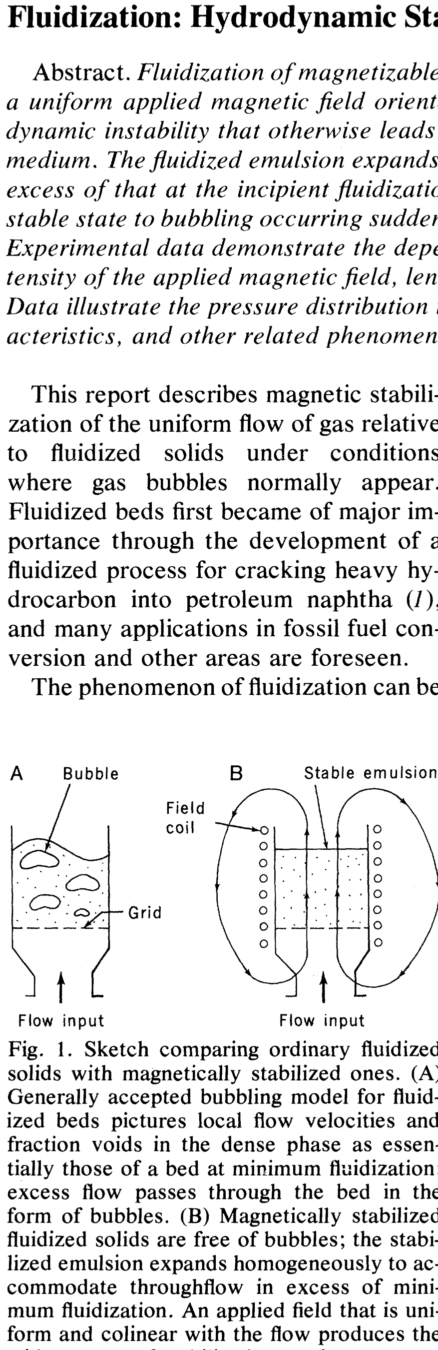

Fig. 1. Sketch comparing ordinary fluidized solids with magnetically stabilized ones. (A) Generally accepted bubbling model for fluidized beds pictures local flow velocities and fraction voids in the dense phase as essentially those of a bed at minimum fluidization; excess flow passes through the bed in the form of bubbles. (B) Magnetically stabilized fluidized solids are free of bubbles; the stabilized emulsion expands homogeneously to accommodate throughflow in excess of minimum fluidization. An applied field that is uniform and colinear with the flow produces the widest range of stabilized operation.

For a gas-fluidized bed in which the gas velocity is greater than the incipient gas velocity, most of the excess gas passes through the bed as bubbles. The bubbles agitate the bed in passing through and promote heat transfer, but some of the gas in the bubbles bypasses the particles altogether, lowering the efficiency of contacting. In addition, the bubbles promote attrition and entrainment of solids, bed slugging (*3*), and uncertainties in process scale-up (*4*).

By providing the solids of the bed with magnetizability and applying a uniform magnetic field that is steady in time and oriented parallel to the direction of gas flow (Fig. 1B), I found that bubble-free fluidized beds are obtained over a substantial range of gas velocities. These

0036-8075/79/0406-0057$00.50/0